Empirical two-band model for quantum wells and superlattices in an electric field

R. P. Leavitt

U.S. Army Laboratory Command, Harry Diamond Laboratories, 2800 Powder Mill Road, Adelphi, Maryland 20783-1197

This paper considers in detail the empirical two-band model formulated by Nelson *et al.* [Phys. Rev. B **35**, 7770 (1987)] for the electronic states of semiconductor quantum wells and superlattices. The model is also extended to the case where the structure of interest is in an external potential. It is shown that one can define probability and probability current densities such that a continuity equation is satisfied and that solutions corresponding to different energies are orthogonal. Expressions are derived for the oscillator strengths of interband transitions and of intersubband transitions within the conduction band. The pair of coupled first-order differential equations resulting from the model can be recast into a single, second-order Schrödinger equation with an energy- and position-dependent effective mass. For a uniform electric field, it is shown that analytic solutions to this equation can be obtained with an error of order $(\gamma F)^2$, where γ is the nonparabolicity parameter and F is the electric field. For a 200-Å rectangular GaAs/Al$_x$Ga$_{1-x}$As quantum well, results are presented for electric-field-dependent conduction-subband energies, envelope functions, interband oscillator strengths, and tunneling resonance widths. These results are compared with the corresponding results obtained by a direct numerical integration of the two-band-model Schrödinger equation and with results obtained using the single-band envelope-function approximation.

I. INTRODUCTION

The most commonly used theoretical models for calculating the electronic properties of quantum wells and superlattices fall into two categories: those based on tight-binding methods (such as Schulman and Chang's empirical tight-binding treatment[1]) and those based on $\mathbf{k} \cdot \mathbf{p}$ perturbation theory.[2] The single-band envelope-function approximation is the simplest example of the latter. Despite a wealth of theoretical treatments that have been discussed to date, very little work has been done to develop models that go beyond the single-band approximation for quantum wells and superlattices in an electric field.

In Kane's eight-band model for bulk semiconductors,[3] the interactions among the conduction band, the light- and heavy-hole bands, and the spin-orbit (split-off) bands are considered within the context of $\mathbf{k} \cdot \mathbf{p}$ perturbation theory. This treatment results in a reasonably simple model for the band structure of a bulk III-V semiconductor near the Γ point that contains a number of adjustable parameters, determined by fitting either to a more precise band-structure calculation or to experimental data (e.g., effective masses determined via cyclotron resonance).

In applying the model to problems involving hetero-junctions, Schuurmans and 't Hooft[4] discovered that the full eight-band Kane description yielded spurious roots. That is, solutions for the square of the wave vector k^2 as a function of the energy E included values of k that were outside the first Brillouin zone, i.e., far outside the range of validity of $\mathbf{k} \cdot \mathbf{p}$ perturbation theory. To rectify this problem, they considered a reduced model in which the conduction and light-hole bands were handled separately, each with its own energy-dependent effective mass. A similar approach was suggested by Pötz, Porod, and Fer-ry[5] who decoupled the eight-band differential equations by neglecting derivatives higher than second order and thereby obtained separate second-order differential equations (with energy-dependent factors) for each band. While these approaches incorporate the major effects of band nonparabolicity, there are difficulties in principle with the use of an energy-dependent effective mass in a model that considers only a single band at a time; specifically, solutions corresponding to different energies are not necessarily orthogonal to each other if the components of the envelope functions for the neglected bands are not accounted for.

Ram-Mohan, Yoo, and Aggarwal[6] proposed a transfer-matrix treatment for energy bands in superlattices that uses all eight bands of Kane's bulk model. It is not clear from this paper, however, how the authors handle the problem of spurious roots discussed above; nevertheless, this method appears to give a good description of electronic states in quantum wells and superlattices. A somewhat different approach to band nonparabolicity is taken by Persson and Cohen[7] and by Ekenberg,[8] who consider an expansion of $E(k)$ in powers of k to obtain a differential equation for the envelope function that is higher than second order. In principle, extra interface conditions are needed as a consequence. However, the authors of these papers side step this issue, and it is not clear that a unique, consistent description can be obtained from this approach.

In this paper, I consider a two-band model that is an empirical version of a coupled conduction-band–light-hole-band model considered by Bastard.[9] In the empirical two-band model, formulated originally by Nelson, Miller, and Kleinman[10] for the zero-field case, the conduction and light-hole bands are considered separately,

and parameters in the model are chosen to match the effective masses and band nonparabolicity parameters determined by other means. Based on the favorable comparison by Yoo, Ram-Mohan, and Nelson[11] of the empirical two-band model with the more sophisticated eight-band transfer-matrix technique[6] and other k·p-based methods, it is clear that the empirical two-band model merits further exploration. Here I consider the properties of the model in more detail and show that the model can easily be extended to calculate energies in the presence of an electric field.

In Sec. II the empirical two-band model (as discussed by Nelson, Miller, and Kleinman[10]) is presented and placed on a firmer footing by the introduction of a "fictitious" band that represents the effects of all the bands that interact with the band of interest. The general properties of solutions to the model are discussed, and appropriate interface conditions for the model are obtained. I show that, in an external potential $V(z)$, the eigenvalue equation can be recast into a single second-order Schrödinger equation with an energy- and position-dependent effective mass. Momentum matrix elements appropriate for optical transitions between valence- and conduction-band states and for transitions within the conduction band are calculated. In Sec. III I show that if $V(z)$ is linear (i.e., the structure of interest is in a uniform electric field) approximate analytic solutions to the model can be obtained with an error of order $(\gamma F)^2$, where γ is the nonparabolicity parameter and F is the electric field. Finally, in Sec. IV the formalism is applied to the calculation of electron-subband-edge energies for a (200 Å GaAs)/Al$_{0.3}$Ga$_{0.7}$As quantum well in an electric field. A comparison of these results using the analytic approximation with a direct numerical integration shows that the former approach is capable of very high accuracy. I also compare results for envelope functions, oscillator strengths for interband transitions, and field-induced tunneling out of the quantum well with corresponding results obtained using the single-band envelope-function approximation.

II. EMPIRICAL TWO-BAND MODEL

A. Physical origin of the model

The specific problem considered in this paper is that of calculating quantum-confined subband-edge energies and related quantities in the presence of an electric field. For concreteness, structures in which the interface normals are along the [001] direction[12] are considered. Thus we may set k_x and k_y equal to zero, and consider the usual reduction of the 8×8 Kane Hamiltonian[3] into a pair of 3×3 matrices representing the interaction of conduction-band (CB), light-hole (LH), and spin-orbit bands with spin up and spin down, respectively, and a pair of 1×1 matrices for the heavy-hole (HH) band. Thus the heavy-hole band becomes parabolic and is not considered in detail here. These simplifications are not possible if $k_\parallel \neq 0$; thus the empirical two-band formalism describes only subband-edge states and is not applicable to properties (such as those of excitons) that depend on

the nature of electronic states away from $k_\parallel = 0$.

Bastard's starting point[9] is to neglect the spin-orbit band entirely, and to write out a 2×2 Hamiltonian representing the interaction of CB and LH bands,

$$H = \begin{bmatrix} E_c + s\varepsilon & \sqrt{2/3}iP_{cv}k \\ -\sqrt{2/3}P_{cv}k & E_v - (\gamma_1 + 2\gamma_2)\varepsilon \end{bmatrix}, \quad (1)$$

where small terms resulting from lack of inversion symmetry[3] have been omitted. In Eq. (1) E_c and E_v are the conduction- and valence-band-edge energies, γ_1 and γ_2 are the "bare" Luttinger parameters, s is a parameter related to the conduction-band effective mass,[4] $\varepsilon = \hbar^2 k^2/2m_e$, m_e is the free-electron mass, and[4]

$$P_{cv} = -\frac{i\hbar}{m_e}\langle s|p_z|z\rangle, \quad (2)$$

where $|s\rangle$ and $|z\rangle$ are state vectors representing, respectively, the Bloch functions at $k=0$ for the conduction band (Γ_1 representation of T_d) and for the z-transforming component of the valence band (Γ_5 representation).

Bastard's simplification[9] of this two-band model arises from neglecting the terms in Eq. (1) containing ε. The motivation is that the contributions of these terms to the effective masses are small and that a second-order differential equation can then be derived, as we shall see, for either the conduction band or the light-hole band alone.[13] For a bulk crystal, we can then solve for the square of the wave vector in terms of the energy:

$$k^2 = \tfrac{3}{2}(E - E_c)(E - E_v)/P_{cv}^2, \quad (3)$$

which may be written in the form

$$E - E_c = \frac{\hbar^2 k^2}{2m(E)}, \quad (4)$$

where the energy-dependent effective mass $m(E)$ is

$$m(E) = \frac{3\hbar^2(E - E_v)}{4P_{cv}^2}. \quad (5)$$

If we write

$$m(E) = m^*\left[1 + \frac{2m^*\gamma(E - E_c)}{\hbar^2}\right], \quad (6)$$

then the conduction-band-edge effective mass is

$$m^* = \frac{3\hbar^2 E_g}{4P_{cv}^2}, \quad (7)$$

and the nonparabolicity parameter for the conduction band is[14]

$$\gamma = \frac{2P_{cv}^2}{3E_g^2} = \frac{\hbar^2}{2m^* E_g}, \quad (8)$$

where $E_g = E_c - E_v$ is the energy gap.

It can be easily shown that, within this simplified two-band model, the effective masses and nonparabolicity parameters for the conduction and light-hole bands are identical and differ significantly from the "true" values.

Nelson, Miller, and Kleinman[10] considered an "empirical" two-band model based on Bastard's formulation in which m^* and γ are chosen separately for each of the bands on an empirical basis. Thus, from Eq. (1), the simplified empirical two-band Hamiltonian for the conduction band is written as

$$H = \begin{bmatrix} E_c & \dfrac{i\hbar^2 k}{2m^*\sqrt{\gamma}} \\ \dfrac{-i\hbar^2 k}{2m^*\sqrt{\gamma}} & E_c - \dfrac{\hbar^2}{2m^*\gamma} \end{bmatrix} . \quad (9)$$

Note that the energy gap in this model, $\hbar^2/2m^*\gamma$, does not coincide (necessarily) with the "true" energy gap, given realistic choices of m^* and γ. In fact one can consider the "light-hole" band in the empirical two-band model as a "fictitious" band $|v'\rangle$ that represents the effects of all the bands that interact with the conduction band. In this case the momentum matrix element P_{cv} defined by Eq. (2) is replaced by an effective matrix element $P_{cv'}$ between the conduction band and the fictitious band. Note also that, although the matrix elements in Eq. (9) diverge as $\gamma \to 0$, the degree of mixing of the conduction and (fictitious) light-hole bands is proportional to $\sqrt{\gamma}k$ and actually vanishes in the limit $\gamma \to 0$. Thus in this limit we recover a parabolic conduction band with an effective mass m^*.

It is interesting to consider the following choice for the wave function of the fictitious light-hole-like band:

$$|v'\rangle = \sum_n \frac{\langle n|p_z|c\rangle \, |n\rangle}{A(E_c - E_n)} . \quad (10)$$

Here, the sum extends over all states except the conduction band $|c\rangle$, and

$$A^2 = \sum_n \frac{|\langle n|p_z|c\rangle|^2}{(E_c - E_n)^2} . \quad (11)$$

It can be easily shown that, if the energy of the fictitious band $E_{v'}$ is chosen such that the effective energy gap is given by

$$E_c - E_{v'} = \sum_n \frac{|\langle n|p_z|c\rangle|^2}{(E_c - E_n)} \Big/ \sum_n \frac{|\langle n|p_z|c\rangle|^2}{(E_c - E_n)^2} , \quad (12)$$

then the wave function for the conduction band given by the model is correct to first order in k, and the effective mass is the same as that given by second-order $\mathbf{k}\cdot\mathbf{p}$ perturbation theory (except that the free-electron contribution to $1/m^*$ is missing). Then the nonparabolicity parameter can be obtained from $\gamma = \hbar^2/2m^*(E_c - E_{v'})$. This fictitious-state construction is not unique, and the value deduced for γ may not be correct; the argument above is given to show one way such a fictitious band may be constructed.

We now introduce an external potential by adding a term $V(z)$ to the diagonal elements of Eq. (9). At the same time, if we replace k by $-id/dz$ in Eq. (9), we obtain the following:

$$H = \begin{bmatrix} E_c + V(z) & \dfrac{\hbar^2}{2m^*\sqrt{\gamma}}\dfrac{d}{dz} \\ -\dfrac{\hbar^2}{2m^*\sqrt{\gamma}}\dfrac{d}{dz} & E_c + V(z) - \dfrac{\hbar^2}{2m^*\gamma} \end{bmatrix} . \quad (13)$$

This is the Hamiltonian for the empirical two-band model for conduction-band states in the presence of an external potential.

B. General properties of solutions

Probability and probability current densities can be defined within the empirical two-band model that satisfy a continuity equation. Consider a two-component wave function

$$\Psi = \begin{bmatrix} f \\ g \end{bmatrix} , \quad (14)$$

which is a solution to the time-dependent Schrödinger equation with H given by Eq. (13). If we define the probability density

$$\rho = \Psi^\dagger\Psi = f^*f + g^*g \quad (15)$$

and the probability current density

$$j = \frac{1}{m_e}\Psi^\dagger p_z\Psi = -\frac{i\hbar}{2m^*\sqrt{\gamma}}(g^*f - f^*g) , \quad (16)$$

then we can write a continuity equation as follows:

$$\frac{d\rho}{dt} + \frac{dj}{dz} = 0 . \quad (17)$$

Furthermore, since H is Hermitian, solutions to the time-independent Schrödinger equation corresponding to different energies are orthogonal (contrary to claims made in Ref. 7). We have

$$\int \Psi_1^\dagger\Psi_2 \, dz = \int (f_1^*f_2 + g_1^*g_2) dz = 0 . \quad (18)$$

Also, we can obtain appropriate boundary conditions by integrating across an interface. We obtain the requirement that the quantity

$$\begin{bmatrix} 0 & \dfrac{\hbar^2}{2m^*\sqrt{\gamma}} \\ -\dfrac{\hbar^2}{2m^*\sqrt{\gamma}} & 0 \end{bmatrix}\Psi \quad (19)$$

be continuous in addition to Ψ itself. The only way that both conditions can be simultaneously satisfied is if the quantity $m^*\sqrt{\gamma}$ is the same on both sides of the interface; if this is the case, both f and g are continuous. This requirement is equivalent to stating that P_{cv} is constant (i.e., independent of the material), which in turn implies that the Bloch functions at $\mathbf{k}=0$ are the same for both materials. Note that these conditions yield continuity of the current, as defined in Eq. (16), across the interface.

In the presence of an external potential, we can define an energy- and position-dependent effective mass as follows:

$$m(E,z)=m^*\left[1+\frac{2m^*\gamma[E-E_c-V(z)]}{\hbar^2}\right] . \quad (20)$$

We can then write the time-independent Schrödinger equation in the following form:

$$\begin{vmatrix} E_c+V(z)-E & \dfrac{\hbar^2}{2m^*\sqrt{\gamma}}\dfrac{d}{dz} \\ -\dfrac{\hbar^2}{2m^*\sqrt{\gamma}}\dfrac{d}{dz} & -\dfrac{\hbar^2}{2m^{*2}\gamma}m(E,z) \end{vmatrix}\begin{bmatrix} f \\ g \end{bmatrix}=0 . \quad (21)$$

The lower component of this equation gives

$$g=-\frac{m^*\sqrt{\gamma}}{m(E,z)}\frac{df}{dz} . \quad (22)$$

Note that, in terms of f alone, the current density becomes

$$j=-\frac{i\hbar}{2m(E,z)}\left[f^*\frac{df}{dz}-f\frac{df^*}{dz}\right] \quad (23)$$

and also that the continuity of g implies that $[1/m(E,z)](df/dz)$ is continuous across an interface. As the nonparabolicity parameter γ approaches zero, we obtain $m(E,z)\rightarrow m^*$, and we recover the usual expressions for j and the interface conditions appropriate for a single-band treatment.

From the upper component of Eq. (21) we can derive a second-order differential equation involving f only:

$$-\frac{\hbar^2}{2}\frac{d}{dz}\left[\frac{1}{m(E,z)}\frac{df}{dz}\right]+V(z)f=(E-E_c)f , \quad (24)$$

where we have used Eq. (22). Again, this equation reduces to the usual single-band effective-mass equation as $\gamma\rightarrow 0$. Note also that, in terms of the "large" components f_1,f_2 of the corresponding wave functions, the orthogonality relation derived above becomes

$$\int\left[f_1^*f_2+\frac{m^{*2}\gamma}{m(E_1,z)m(E_2,z)}\frac{df_1^*}{dz}\frac{df_2}{dz}\right]dz=0 . \quad (25)$$

The erroneous conclusion stated in Ref. 7 regarding the orthogonality of solutions in the two-band model was deduced as a result of the authors' neglect of the second term in Eq. (25).

The arguments presented above between Eqs. (9) and (25) can be repeated for the light-hole band (with different choices of m^* and γ), in which one invokes a "fictitious" conduction-band state $|c'\rangle$ that represents the effects of all other bands that interact with the light-hole band. In this case, one can convert from an "electron" problem to a "hole" problem in the usual fashion by (a) replacing E_c by $E_v+\hbar^2/(2m^*\gamma)$ in Eq. (13), (b) measuring energies downward from the bottom of the valence band (i.e., replacing $E-E_v$ by E_v-E), (c) changing the sign of the potential $V(z)$ (appropriate for the positively charged holes), and (d) taking the complex conjugate of the envelope functions. One then obtains all the results of Sec. II B [with E_c replaced by E_v and $V(z)$ replaced by $-V(z)$], where f is now interpreted as the "large" com-

ponent of the light-hole wave function and γ is interpreted in terms of the momentum matrix element $P_{c'v}$ between the light-hole band $|l\rangle$ and the fictitious conduction band $|c'\rangle$.

C. Momentum matrix elements

Let us now consider optical transitions between eigenstates of the empirical two-band Hamiltonian for various bands. In so doing, we now must keep track of the three actual bands of interest (the conduction band c, the light-hole band l, and the heavy-hole band h, which is assumed to be parabolic), as well as the two fictitious bands v' (which interacts with the conduction band in the model) and c' (which interacts with the light-hole band). I give the results for matrix elements of the momentum operator between two-band-model solutions for transitions between light- and heavy-hole valence-band states and conduction-band states, as well as for transitions within the conduction band. Note that the empirical two-band formalism applies only to transitions between subband-edge states (i.e., $k_\parallel$ is set to zero). Our results are therefore not applicable to excitonic transitions or to transitions in which anomalous parallel dispersion of subbands plays an important role.[15]

The results presented here are expressed in terms of the "large" components of the appropriate two-band model solutions, i.e., in terms of the appropriate solutions to Eq. (24). In what follows the magnetic quantum numbers M for the various states are suppressed; it is understood that these quantum numbers are chosen to satisfy the selection rules $\Delta M=0$ for p_z transitions (light polarized along the quantization axis) and $\Delta M=1$ for p_1 transitions (light polarized in the plane of the layers). Using the momentum matrix elements (and phase conventions) given in the Appendix, we arrive at the following. For a light-hole to conduction-band transition,

$$\langle c|p_z|l\rangle=\sqrt{2/3}\frac{im_e}{\hbar}P_{cv}$$

$$\times\int\left[f_c^*f_l-r\frac{m_c^*m_l^*\sqrt{\gamma_c\gamma_l}}{m_c(E_c,z)m_l(E_1,z)}\right.$$

$$\left.\times\frac{df_c^*}{dz}\frac{df_l}{dz}\right]dz \quad (26)$$

and

$$\langle c|p_1|l\rangle=-\sqrt{1/3}\frac{im_e}{\hbar}P_{cv}$$

$$\times\int\left[f_c^*f_l+r\frac{m_c^*m_l^*\sqrt{\gamma_c\gamma_l}}{m_c(E_c,z)m_l(E_l,z)}\right.$$

$$\left.\times\frac{df_c^*}{dz}\frac{df_l}{dz}\right]dz , \quad (27)$$

where r is the ratio of momentum matrix elements: $r=P_{c'v'}/P_{cv}$. ($P_{c'v'}$ is the momentum matrix element between the fictitious conduction band and the fictitious light-hole band.) The primary difficulty with the above

expressions is that the quantity r is not known. However, we would expect that the largest component of the fictitious state $|c'\rangle$ is the true conduction-band state $|c\rangle$ and that, similarly, $|v\rangle$ is the largest component of $|v'\rangle$ (i.e., $\langle c'|c\rangle$ and $\langle v'|v\rangle$ are close to unity). Thus we can argue that r is close to unity. Furthermore, the terms involving r generally make small contributions to the momentum matrix elements. Thus we can set $r=1$ in Eqs. (26) and (27) without considerable error in the matrix elements. As γ_c and γ_v approach zero, Eqs. (26) and (27) reduce to the usual single-band effective-mass expressions.

For a heavy-hole to conduction-band transition, we simply obtain $\langle c|p_z|h\rangle=0$ (as in the single-band case) and

$$\langle c|p_1|h\rangle=-\frac{im_e}{\hbar}P_{cv}\int f_c^* f_h dz \ . \tag{28}$$

Finally, consider transitions between two conduction-band states c_2 and c_1. We find

$$\langle c_2|p_z|c_1\rangle=-\frac{im_e\hbar}{2}\int\left[[m(E_1,z)]^{-1}f_2^*\frac{df_1}{dz}\right.$$
$$\left.-[m(E_2,z)]^{-1}\frac{df_2^*}{dz}f_1\right]dz \tag{29}$$

and

$$\langle c_2|p_1|c_1\rangle=\frac{im_e\hbar}{2\sqrt{2}}\int\left[[m(E_1,z)]^{-1}f_2^*\frac{df_1}{dz}\right.$$
$$\left.+[m(E_2,z)]^{-1}\frac{df_2^*}{dz}f_1\right]dz \ . \tag{30}$$

Equation (29) reduces to the expected result[16] in the limit of parabolic bands. On the other hand, no analog to Eq. (30) is obtained in a single-band model (in which $\langle c_2|p_1|c_1\rangle=0$); it predicts intersubband transitions in quantum-well structures with light polarized in the plane of the layers. This is, to my knowledge, a new result.

We can also calculate matrix elements of $\mathbf{p}$ between valence-band states; however, since the empirical two-band model does not account for the full structure of the valence band, these matrix elements do not give correct results in the limit of vanishing nonparabolicity. (For the correct results in this limit, see, for example, Ref. 16.)

III. APPROXIMATE SOLUTIONS
IN A UNIFORM ELECTRIC FIELD

Consider the case for which the external potential $V(z)$ is linear in z; i.e., the structure of interest is in a uniform electric field F, with $V(z)=-eFz$. The following argument shows that one can obtain approximate solutions to the second-order differential equation, Eq. (24), that are accurate provided that γF is small.

Let us first examine the case of an arbitrary potential $V(z)$. Let the function $f_0(z_0+u)$ be a solution to the

differential equation

$$-\frac{\hbar^2}{2m_0}\frac{d^2f_0}{du^2}+[V(u+z_0)-V(z_0)]f_0=E_0f_0 \ , \tag{31}$$

which is the ordinary single-band envelope-function equation with an effective mass m_0. Our approach will be to obtain solutions to the two-band differential equation, (24), by choosing a function similar to $f_0(u)$ except that its amplitude and argument are slowly modulated. Specifically, we seek an approximate solution to Eq. (24) of the form

$$f(z)=A(u)f_0\left[z_0+\int_0^u B(u')du'\right] \ , \tag{32}$$

where $A(u)$ and $B(u)$ are taken to be slowly varying, with $A(0)=B(0)=1$, and where we identify

$$m_0=m(E,z_0)=m^*\left[1+\frac{2m^*\gamma E_0}{\hbar^2}\right] \ , \tag{33}$$

where E_0 is chosen as

$$E_0=E-E_c-V(z_0) \ , \tag{34}$$

and where $u=z-z_0$, z_0 being an arbitrarily chosen point at which the functions f and f_0 are taken to coincide.

If we substitute the approximate solution $f(z)$ given by Eq. (32) into the differential equation, Eq. (24), we obtain the following:

$$-\frac{\hbar^2}{2m}B^2f_0''-\frac{\hbar^2}{2m}\left[B'+\frac{2A'}{A}B-\frac{m'B}{m}\right]f_0'$$
$$-\left[\frac{\hbar^2}{2m}\left[\frac{A''}{A}-\frac{m'A'}{mA}\right]\right.$$
$$\left.+V(z_0)-V(u+z_0)+E_0\right]f_0=0 \ . \tag{35}$$

Here m is $m(E,z)$ as defined in Eq. (20). In the above, the primes on A and B indicate differentiation with respect to the variable u, whereas those on f_0 indicate differentiation with respect to its full argument. If we now neglect the A'' and $m'A'$ terms, Eqs. (31) and (35) become identical, provided

$$B=\left[\frac{m}{m_0}\right]^{1/2} \tag{36}$$

and

$$A=\left[\frac{m}{m_0}\right]^{1/4} \ . \tag{37}$$

With these choices, the term multiplying f_0' in Eq. (35) vanishes identically.

The neglected quantity multiplying f_0 in Eq. (35) can be written as

$$\frac{\hbar^2}{2m}\left[\frac{A''}{A}-\frac{m'A'}{mA}\right]=\frac{\hbar^2(4mm''-7m'^2)}{32m^3}$$

$$=-\frac{m^{*2}\gamma}{8m^3}\left[2mV''+\frac{7m^{*2}\gamma V'^2}{\hbar^2}\right].$$

$$(38)$$

This result reveals why the approximations made above are particularly appropriate for a uniform electric field. For an arbitrary potential, both terms in Eq. (38) are nonzero, and the error in the approximate solution obtained is of order γ and increases with the strength of the potential; the approximate solution is therefore not usable. For a linear potential, on the other hand, the first term is zero, and the error in the approximate solution is of order $(\gamma F)^2$. We can obtain a rough condition for the validity of this approximation by requiring that this error be small in comparison with energies characteristic of the structure under consideration. Setting $V(z)=-eFz$ and neglecting factors of order unity, we obtain

$$\gamma F \ll \frac{\hbar}{e}\left[\frac{|E_{\rm char}|}{m^*}\right]^{1/2}.$$

$$(39)$$

A rough estimate for the confinement energy in a region of thickness L is $E_{\rm char}=\hbar^2\pi^2/(2m^*L^2)$. Using this in Eq. (39) and again neglecting factors of order unity, we obtain

$$eFL \ll \frac{\hbar^2}{2m^*\gamma},$$

$$(40)$$

which states that the potential drop across the region of interest must be small in comparison with the effective energy gap. For example, given that $m^*=0.08m_e$ and $\gamma=80$ Å^2 (an excessively large value), we require $L \ll 600$ Å if $F=100$ kV/cm.

In applying this approximation to a real layered semiconductor structure, one must divide the structure into a number of physical regions within which the condition (40) is valid. Normally, these regions can be chosen to coincide with the layers comprising the structure, but on occasion (e.g., for abnormally wide quantum wells or large electric fields) one must further subdivide certain regions to assure that Eq. (40) holds within each region. In each region, the solution is written as a linear combination of the two usual Airy-function solutions[17] to Eq. (31), Ai and Bi, which are then modified in accordance with Eq. (32). In so doing, one chooses the parameter z_0 as the value of the coordinate z in the center of the region. For semi-infinite boundary layers, one chooses z_0 as the value of z at the boundary. From this point on, the implementation is essentially identical to that for a single-band envelope-function problem. A transfer-matrix method can be used to propagate solutions from one region to the next, using the matching conditions given by Eq. (19). The fact that there are no true eigenstates in an electric field for finite potential barriers might present difficulty, but methods that have been devised previously to deal with this problem in the context of the

single-band envelope-function method[18,19] can be carried over directly to the empirical two-band model.

IV. APPLICATIONS OF THE MODEL

I now consider applications of the model to quantum-well structures. For simplicity, I consider only a 200-Å rectangular GaAs/Al$_{0.3}$Ga$_{0.7}$As quantum well; other, more complex layered structures, as well as comparisons with experimental data, will be dealt with in future publications. Effective masses (in units of the bare electron mass) are taken to be 0.067 for GaAs (Ref. 20) and 0.0919 for Al$_{0.3}$Ga$_{0.7}$As.[21] The conduction-band offset between the well and barrier materials is 302 meV, which is 70% of the band-gap difference (as given in Ref. 22). For GaAs, the value $\gamma=40$ Å^2 is used, which is representative of values used previously.[10,11,23] For Al$_{0.3}$Ga$_{0.7}$As, $\gamma=21.3$ Å^2, which is obtained from the interface conditions (see Sec. II B).

Results for the five conduction-subband-edge levels of the 200-Å well as functions of the electric field are shown in Fig. 1. The solid lines represent the results of the analytic approximation to the two-band model. The dashed lines are corresponding results calculated in the single-band approximation. In both cases, the methods of Aus-
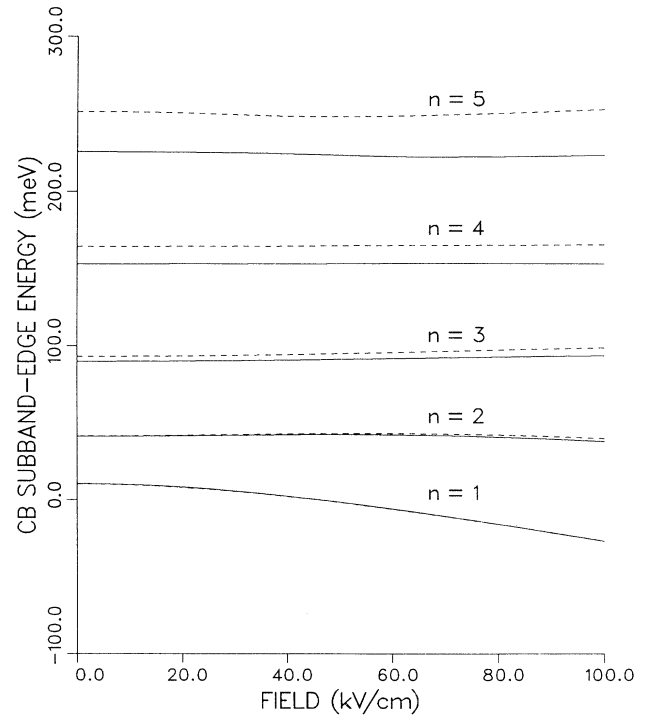
FIG. 1. Electron-subband-edge energies for a (200 Å GaAs)/Al$_{0.3}$Ga$_{0.7}$As quantum well as functions of electric field, calculated using the analytic approximation to the empirical two-band model (solid lines) and the single-band envelope-function approximation (dashed lines). The zero of energy is taken as the conduction-band-edge energy at the center of the well.

R. P. LEAVITT

tin and Jaros[18] were used to deal with the fact that there are no true eigenstates of the Hamiltonian in an electric field due to the finite probability of field-induced tunneling out of the well. As pointed out previously for the zero-field case,[10] the energy obtained for the ground state in the two-band model is slightly higher than the single-band result, whereas for the excited states the two-band-model energies are lower than the single-band-model energies. These results are easily understood in terms of the changes in the energy-dependent effective masses of the well and barrier materials with energy and the probability of finding the electron in the barrier.[10] As expected, deviations from the single-band results are most pronounced for the higher-energy states. For the most part, however, the electric-field dependence of the energy in the two-band model follows that of the single-band calculation very well.

To give an idea of the actual error made in the analytic
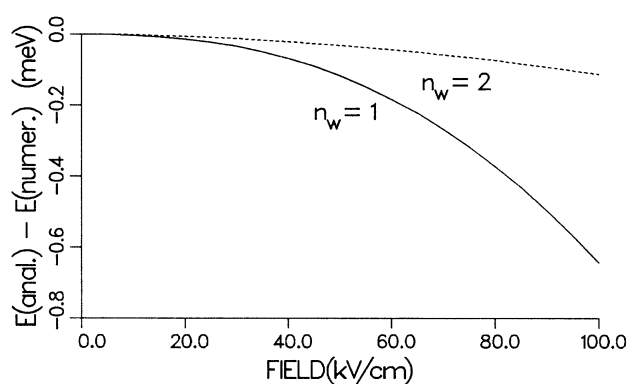
(a)
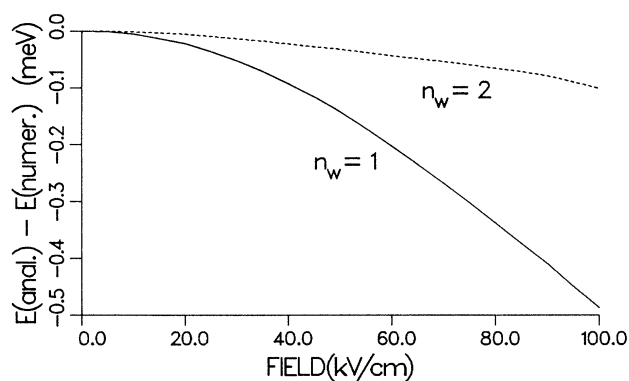
(b)

FIG. 2. (a) Difference between ground-state energies for the 200-Å quantum well calculated using the analytic approximation and the numerical solution to Eq. (24) as a function of electric field. For $n_w = 1$, the well was considered a single layer; for $n_w = 2$, the well was divided into two 100-Å regions. (b) Similar to (a), but for the $n = 3$ conduction-subband-edge energy.

approximation to the two-band model, the energies of the 200-Å well were calculated as functions of electric field by direct numerical integration of the Schrödinger equation, Eq. (24). Figure 2(a) shows the difference between the ground-state energies calculated with the analytic approximation and with the numerical integration. For the solid curve, the quantum well was considered to be a single layer in the analytical approximation. For the dashed curve, the quantum well was divided into two 100-Å layers. [Based on Eq. (40), I would expect the latter calculation to be more accurate.] In both cases, the difference between analytic and numerical energies is well within 1 meV. Dividing the quantum well in half improves the accuracy of the analytic approximation for high electric fields by better than a factor of 5. As the number of layers into which the well is divided is increased further, the analytic results rapidly approach the numerical results. Similar results are obtained for the $n = 3$ level; these results are shown in Fig. 2(b). As a test of the methods used, the calculations were repeated with $\gamma = 0$; in this case the energies obtained analytically and numerically agreed to much better than 0.001 meV. Thus the energy differences shown in Fig. 2 are indicative of the error made in the analytic approximation to the two-band model and are not, e.g., the result of numerical errors.

Figure 3(a) shows the conduction-band diagram for the 200-Å quantum well with an electric field of 50 kV/cm. Also shown are the two components of the two-band en-

(a)

(b)
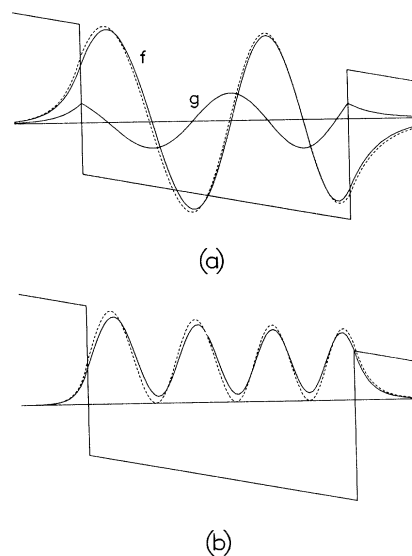
FIG. 3. (a) Conduction-band diagram for a 200-Å quantum well with an electric field of 50 kV/cm. Also shown are the two components f and g of the two-band envelope function (solid lines) and the single-band envelope function (dashed line) for the $n = 4$ subband of the well. The horizontal line shows the $n = 4$ subband-edge energy and serves as a zero for the envelope functions. (b) Corresponding probability densities, calculated using the two-band model (solid line) and the single-band model (dashed line).

velope function (solid lines) and the single-band envelope function (dashed line) for the $n = 4$ subband of the well. The horizontal line shows the subband-edge energy for this level and also serves as a zero for the envelope functions. In Fig. 3(b) the corresponding probability densities for the two-band model (solid line) and the single-band model (dashed line) are compared. While the two probability densities are similar, the probability density for the two-band model has no zeros within the well. This feature is characteristic of any multiband effective-mass treatment of quantum wells and superlattices.

I have also calculated the transition matrix elements for electron-hole transitions between the various conduction-band and light- and heavy-hole subbands according to Eqs. (26)–(28). Figure 4(a) shows the squares of the matrix elements for certain $\Delta n \neq 0$ HH-CB transitions given by Eq. (28) [without the factor $(m_e P_{cv}/\hbar)^2$] as solid lines. For comparison, the corresponding results from a single-band effective-mass calculation are shown. Similarly, Fig. 4(b) shows the squares of the matrix elements for LH-CB transitions given by Eq. (27) [without the factor $(m_e P_{cv}/\hbar)^2/3$]. These quantities are proportional to the oscillator strengths for light polarized parallel to the confining layers. For the $\Delta n = 0$ transitions (not shown), there is very little difference between the two-band results and the single-band results. Even for the
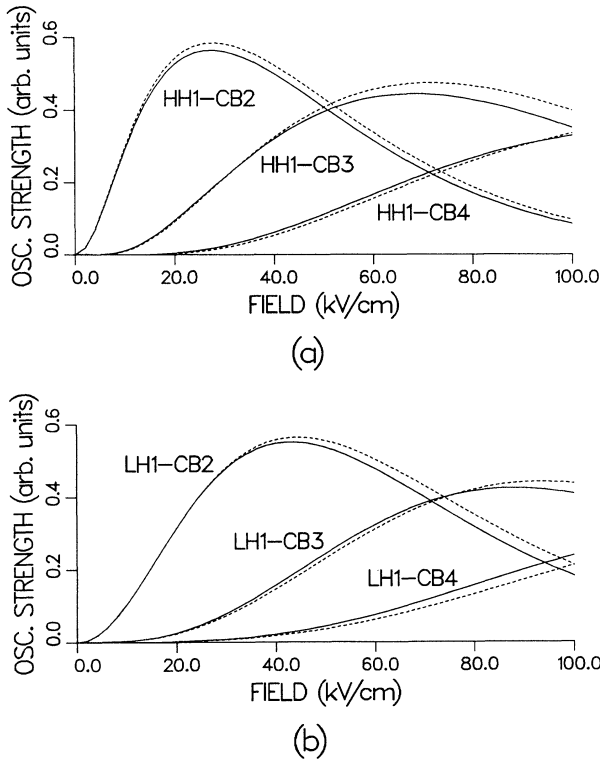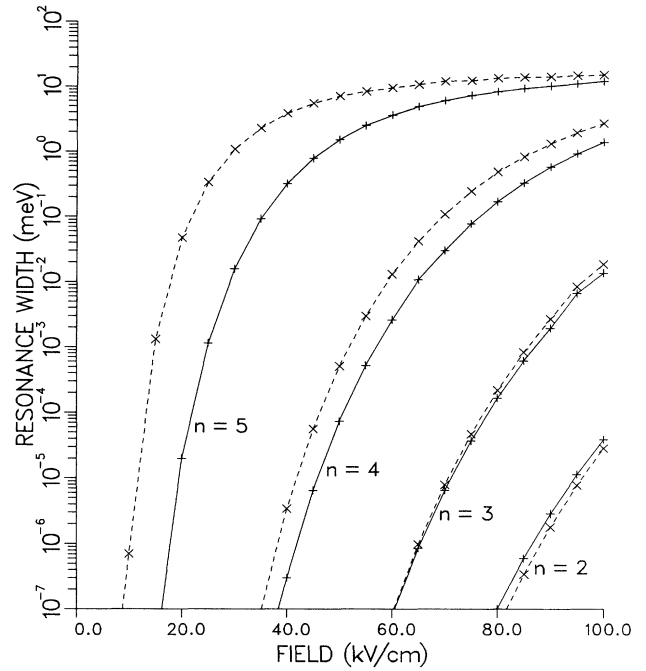
FIG. 5. Resonance widths [arising from field-induced tunneling (Ref. 21)] for excited conduction-band states of the 200-Å quantum well as functions of electric field. Solid lines, results of the analytic approximation to the empirical two-band model; dashed lines, results of the single-band envelope-function approximation.

$\Delta n \neq 0$ transitions, the differences between the two sets of calculations are minor; thus the oscillator strengths are not very sensitive to the presence of nonparabolicity.

To further illustrate the effects of nonparabolicity on the electric-field dependence of the quantum-well levels, Fig. 5 shows the calculated resonance widths as functions of field for each of the excited states of the 200-Å well. These widths are obtained naturally in the phase-shift method as the full widths at half maximum of the calculated densities of states and are proportional to the transition rates for field-induced tunneling out of the quantum well.[24] In Fig. 5, solid lines are the two-band results and dashed lines correspond to the single-band approximation. Large differences between the two models are apparent; for the $n = 5$ and 4 states, these differences arise primarily because of the differences in the calculated energies obtained in the two models. For the $n = 2$ state, the tunneling rate is actually larger in the two-band model than in the single-band model, even though the calculated energy is slightly lower. This is because the effective mass in the $Al_{0.3}Ga_{0.7}As$ barrier decreases as the energy decreases below the $Al_{0.3}Ga_{0.7}As$ conduction-band edge, which enhances the tunneling probability.

V. CONCLUSION

I have studied in detail the properties of an empirical two-band model for the electronic structure of quantum

(a)

(b)

FIG. 4. (a) Oscillator strengths for certain $\Delta n \neq 0$ HH-CB transitions in the 200-Å quantum well as functions of electric field, with light polarized parallel to the layers. Solid lines, two-band results; dashed lines, single-band results. (b) Corresponding results for LH-CB transitions.

wells and superlattices. The general properties of solutions to the model were examined in an arbitrary external potential $V(z)$. Within the model, one can define probability and probability current densities such that a continuity equation is obeyed. Also, solutions to the time-dependent Schrödinger equation corresponding to different energies are orthogonal, contrary to the claims of Persson and Cohen.[7] Momentum matrix elements for interband and intersubband transitions were calculated, and the pair of first-order differential equations resulting from the model was recast into an effective second-order Schrödinger equation with an energy- and position-dependent effective mass.

For the case where $V(z)$ is linear, an approximate solution to this equation was obtained in which solutions to the corresponding single-band effective-mass equation are modulated by slowly varying functions. In other words, in this approximation the effect of the position dependence of the effective mass is to distort the single-band solutions. As an example of an application, the conduction-subband-edge energies for a (200 Å GaAs)/$Al_{0.3}Ga_{0.7}As$ quantum well were calculated as functions of the electric field and compared with corresponding results based on the single-band envelope-function approximation. The high accuracy of the analytic approximation was verified by comparing these results with the results of numerical integration of the effective Schrödinger equation. Envelope functions and oscillator strengths for interband transitions were calculated using the two-band model and compared with corresponding results obtained from a single-band calculation. I showed large differences in the calculated rates for field-induced tunneling out of the quantum well obtained from the two-band and single-band models.

There are few cases in the literature in which nonparabolicity effects have been incorporated into quantum-well calculations in an electric field. Stevens et al.[25] replaced the linear potential with a large number of steps in which the potential is constant and used an energy-dependent (but position-independent) effective mass in each step. While such an approach can, in principle, give good results, the number of steps required to do so may be very large. In a simpler treatment, Campi and Alibert[26] retained the linear potential, but used an effective mass that was energy dependent but constant in each layer. In my opinion, this approach will lead to incorrect results for the electric-field dependence of the subband-edge energies.

The results presented here are easy to incorporate into a computer code for calculating quantum-well and superlattice subband energies, since they use the well-known solutions for the single-band envelope functions in an electric field. Insofar as the accuracy of the model is concerned (in comparison with more exact and sophisticated treatments), we can rely on the comparison by Yoo, Ram-Mohan, and Nelson[11] (at zero electric field) of the empirical two-band model results with the results of a full eight-band calculation.[6] In Ref. 11, conduction-subband-edge energies obtained from these models agreed to considerably better than 1 meV for a wide range of quantum-well widths; the light-hole subband-edge ener-

gies agreed to about 4 meV, for the most part. These differences are considerably smaller than the shifts arising from nonparabolicity, and so the empirical two-band model should give a good first-order account of these effects. Also, the two-band model accounts well for the so-called mass renormalization effect in the $Al_xGa_{1-x}As$ barriers which was experimentally demonstrated by Brozak et al.[27] Thus the model should be a good one for studying effects of coupling between two or more quantum wells on the electronic and optical properties of such coupled systems.

ACKNOWLEDGMENTS

APPENDIX: BASIS STATES AND MOMENTUM MATRIX ELEMENTS

In the following, I show how representations of the double group can be constructed from those of the single groups. Throughout the discussion, I use the isomorphism between representations of the T_d and O_h point groups and those of the full rotation group R_3. Thus the notation $|s\rangle$ is used to represent a basis function for the conduction band (Γ_1 representation of T_d) and $|x\rangle$, $|y\rangle$, $|z\rangle$ as basis functions for the valence band (Γ_5 representation). Where there exist corresponding representations of the point group and the rotation group, phases are chosen in such a way that the Condon and Shortley phase convention[28] usually invoked in connection with rotation-group representations is valid also for the point-group representations. For the double-group representations, $|J,M\rangle$-type basis states are chosen, with $J=\frac{1}{2}$ for Γ_6 and Γ_7 and $J=\frac{3}{2}$ for Γ_8. I assume that these latter states are constructed from the single-group representations as follows:

$$|\Gamma_j,M\rangle = \sum_{\mu} C(L,\tfrac{1}{2},J;M-\mu,\mu)|\Gamma_l,M-\mu\rangle |\tfrac{1}{2},\mu\rangle \, ,$$

$$(A1)$$

where, in the above, the Γ_6 state has $L=0$ (Γ_1 single-group representation) and $J=\frac{1}{2}$; the Γ_7 and Γ_8 states have $L=1$ (Γ_5 single-group representation), with $J=\frac{1}{2}$ and $\frac{3}{2}$, respectively.

Writing the states out in full produces the following basis functions for the single-group representations:

$$|\Gamma_1,M=0\rangle = |s\rangle \, ,$$

$$(A2)$$

$$|\Gamma_5, M\rangle = \begin{cases} -\frac{1}{\sqrt{2}}(|x\rangle + i|y\rangle), & M = 1 \\ |z\rangle, & M = 0 \\ \frac{1}{\sqrt{2}}(|x\rangle - i|y\rangle), & M = -1 \end{cases} \qquad \text{(A3)}$$

and for the double-group representations we obtain, for the conduction band,

$$|\Gamma_6, M\rangle = \begin{cases} |s\uparrow\rangle, & M = +\frac{1}{2} \\ |s\downarrow\rangle, & M = -\frac{1}{2}, \end{cases} \qquad \text{(A4)}$$

for the split-off band

$$|\Gamma_7, M\rangle = \begin{cases} -\frac{1}{\sqrt{3}}(|z\uparrow\rangle + |x\downarrow\rangle + i|y\downarrow\rangle), & M = +\frac{1}{2} \\ \frac{1}{\sqrt{3}}(|z\downarrow\rangle - |x\uparrow\rangle + i|y\uparrow\rangle), & M = -\frac{1}{2}, \end{cases} \qquad \text{(A5)}$$

and for the light-hole ($|M| = 1/2$) and heavy-hole ($|M| = 3/2$) bands

$$|\Gamma_8, M\rangle = \begin{cases} -\frac{1}{\sqrt{2}}(|x\uparrow\rangle + i|y\uparrow\rangle), & M = +\frac{3}{2} \\ \sqrt{2/3}|z\uparrow\rangle - \sqrt{1/6}(|x\downarrow\rangle + i|y\downarrow\rangle), & M = +\frac{1}{2} \\ \sqrt{2/3}|z\downarrow\rangle + \sqrt{1/6}(|x\uparrow\rangle - i|y\uparrow\rangle), & M = -\frac{1}{2} \\ \frac{1}{\sqrt{2}}(|x\downarrow\rangle - i|y\downarrow\rangle), & M = -\frac{3}{2}. \end{cases} \qquad \text{(A6)}$$

(Note that the notation here differs from that of the main text in that the group representations are displayed explicitly. These are to be understood implicitly in the main text.)

We can now write all the relevant matrix elements of the momentum operator in terms of the quantity P_{cv} defined by Eq. (2):

$$\langle \Gamma_6, +\tfrac{1}{2}|p_z|\Gamma_7, +\tfrac{1}{2}\rangle = -\langle \Gamma_6, -\tfrac{1}{2}|p_z|\Gamma_7, -\tfrac{1}{2}\rangle$$
$$= -\sqrt{1/3}\frac{im_e}{\hbar}P_{cv}, \qquad \text{(A7)}$$

$$\langle \Gamma_6, +\tfrac{1}{2}|p_z|\Gamma_8, +\tfrac{1}{2}\rangle = \langle \Gamma_6, -\tfrac{1}{2}|p_z|\Gamma_8, -\tfrac{1}{2}\rangle$$
$$= \sqrt{2/3}\frac{im_e}{\hbar}P_{cv}, \qquad \text{(A8)}$$

$$\langle \Gamma_6, +\tfrac{1}{2}|p_1|\Gamma_7, -\tfrac{1}{2}\rangle = -\langle \Gamma_6, -\tfrac{1}{2}|p_{-1}|\Gamma_7, +\tfrac{1}{2}\rangle$$
$$= \sqrt{2/3}\frac{im_e}{\hbar}P_{cv}, \qquad \text{(A9)}$$

$$\langle \Gamma_6, +\tfrac{1}{2}|p_1|\Gamma_8, -\tfrac{1}{2}\rangle = \langle \Gamma_6, -\tfrac{1}{2}|p_{-1}|\Gamma_8, +\tfrac{1}{2}\rangle$$
$$= -\sqrt{1/3}\frac{im_e}{\hbar}P_{cv}, \qquad \text{(A10)}$$

$$\langle \Gamma_6, +\tfrac{1}{2}|p_{-1}|\Gamma_8, +\tfrac{3}{2}\rangle = \langle \Gamma_6, -\tfrac{1}{2}|p_1|\Gamma_8, -\tfrac{3}{2}\rangle$$
$$= -\frac{im_e}{\hbar}P_{cv}, \qquad \text{(A11)}$$

where

$$p_{\pm 1} = \mp \frac{1}{\sqrt{2}}(p_x \pm ip_y). \qquad \text{(A12)}$$

[1]J. N. Schulman and Y.-C. Chang, Phys. Rev. B 31, 2056 (1985).

[2]For a recent review of these and other electronic-structure methods for quantum wells and superlattices, see D. L. Smith and C. Mailhiot, Rev. Mod. Phys. 62, 173 (1990).

[3]E. O. Kane, J. Phys. Chem. Solids 1, 249 (1957).

[4]M. F. H. Schuurmans and G. W. 't Hooft, Phys. Rev. B 31, 8041 (1985); R. Eppenga, M. F. H. Schuurmans, and S. Colak, ibid. 36, 1554 (1987).

[5]W. Pötz, W. Porod, and D. K. Ferry, Phys. Rev. B 32, 3868 (1985).

[6]L. R. Ram-Mohan, K. H. Yoo, and R. L. Aggarwal, Phys. Rev. B 38, 6151 (1988).

[7]A. Persson and R. M. Cohen, Phys. Rev. B 38, 5568 (1988).

[8]U. Ekenberg, Phys. Rev. B 36, 6152 (1987).

[9]G. Bastard, Phys. Rev. B 24, 5693 (1981); 25, 7584 (1982). A three-band model including the split-off band has been considered also; see, for example, G. Bastard and J. A. Brum, IEEE J. Quantum Electron. QE-22, 1625 (1986). This model reduces to a single second-order differential equation for the conduction-band envelope function. However (in contrast with the two-band model), a similar reduction cannot be effected for the light-hole band in this model.

[10]D. F. Nelson, R. C. Miller, and D. A. Kleinman, Phys. Rev. B 35, 7770 (1987).

[11]K. H. Yoo, L. R. Ram-Mohan, and D. F. Nelson, Phys. Rev. B 39, 12 808 (1989).

[12]This approach should work well also for structures quantized along the [111] direction, since in this case the heavy-hole band has symmetry different from that of the light-hole and conduction bands, as is the case for the [001] direction.

[13]In contrast, see S. R. White and L. J. Sham, Phys. Rev. Lett. 47, 879 (1981). In this work the ε terms are retained, and the resulting model contains wing-band solutions that are the analog of the spurious solutions of Ref. 3.

[14]The quantity γ is the coefficient of the first nonparabolic term in the expansion of the effective mass in powers of k^2: $m(k) = m^*(1 + \gamma k^2 + \cdots)$.

[15]Y.-C. Chang and J. N. Schulman, Phys. Rev. B 31, 2069 (1985).

[16]Y.-C. Chang and R. B. James, Phys. Rev. B 39, 12 672 (1989).

[17]H. A. Antosiewicz, in Handbook of Mathematical Functions, Natl. Bur. Stand. Appl. Math. Ser. No. 55, edited by M. Abramowitz and I. A. Stegun (U.S. GPO, Washington, DC, 1964), p. 435.

[18]E. J. Austin and M. Jaros, Phys. Rev. B 31, 5569 (1985).

[19]D. Ahn and S. L. Chuang, Phys. Rev. B 34, 9034 (1986).

[20]P. Lawaetz, Phys. Rev. B 4, 3460 (1971).

[21]Obtained by linear interpolation using the conduction-band effective mass for AlAs given in H. C. Casey, Jr. and M. B. Panish, Heterostructure Lasers, Part B: Materials and Operat-

ing Characteristics (Academic, New York, 1978).

[22] D. Huang, G. Ji, U. K. Reddy, H. Morkoc, F. Xiong, and T. A. Tombrello, J. Appl. Phys. **63**, 5447 (1988).

[23] For a comparison of different nonparabolicity parameters for GaAs, see U. Ekenberg, Phys. Rev. B **40**, 7714 (1989). Note that the value of γ obtained from Ref. 7 is extremely small. See also J. S. Blakemore, J. Appl. Phys. **53**, R123 (1982).

[24] E. J. Austin and M. Jaros, Appl. Phys. Lett. **47**, 274 (1985).

[25] P. J. Stevens, M. Whitehead, G. Parry, and K. Woodbridge, IEEE J. Quantum Electron **QE-24**, 2007 (1988).

[26] D. Campi and C. Alibert, Appl. Phys. Lett. **55**, 454 (1989).

[27] G. Brozak, E. A. de Andrada e Silva, L. J. Sham, F. DeRosa, P. Miceli, S. A. Schwartz, J. P. Harbison, L. T. Florez, and S. J. Allen, Jr., Phys. Rev. Lett. **64**, 471 (1990).

[28] E. U. Condon and G. H. Shortley, *Theory of Atomic Spectra* (Cambridge University Press, London, 1935).